Journal of Solid State Chemistry 181 (2008) 1744–1752

Contents lists available at ScienceDirect

Journal of Solid State Chemistry

journal homepage: www.elsevier.com/locate/jssc

Solid-state ^{27}Al and ^{29}Si NMR characterization of hydrates formed in calcium aluminate–silica fume mixtures

P. Pena [a], J.M. Rivas Mercury [a,1], A.H. de Aza [a,*], X. Turrillas [b], I. Sobrados [c], J. Sanz [c]

[a] Instituto de Cerámica y Vidrio, C.S.I.C., C/ Kelsen, 5, 28049 Cantoblanco-Madrid, Spain
[b] Instituto de Ciencias de la Construcción Eduardo Torroja, C.S.I.C., C/ Serrano Galvache, 4, 28032 Madrid, Spain
[c] Instituto de Ciencia de Materiales, C.S.I.C., C/ Sor Juana Inés de la Cruz, 3, 28049 Cantoblanco-Madrid, Spain

ARTICLE INFO

Article history:
Received 11 September 2007
Received in revised form
26 February 2008
Accepted 22 March 2008
Available online 29 March 2008

Keywords:
Cement and concretes
Si–hydrogarnet
Gibbsite
^{27}Al MAS–NMR
^{29}Si MAS–NMR
Neutron diffraction

ABSTRACT

Partially deuterated $Ca_3Al_2(SiO_4)_y(OH)_{12-4y}$–$Al(OH)_3$ mixtures, prepared by hydration of $Ca_3Al_2O_6$ (C_3A), $Ca_{12}Al_{14}O_{33}$ ($C_{12}A_7$) and $CaAl_2O_4$ (CA) phases in the presence of silica fume, have been characterized by ^{29}Si and ^{27}Al magic-angle spinning–nuclear magnetic resonance (MAS–NMR) spectroscopies. NMR spectroscopy was used to characterize anhydrous and fully hydrated samples. In hydrated compounds, $Ca_3Al_2(OH)_{12}$ and $Al(OH)_3$ phases were detected. From the quantitative analysis of ^{27}Al NMR signals, the $Al(OH)_3/Ca_3Al_2(OH)_{12}$ ratio was deduced. The incorporation of Si into the katoite structure, $Ca_3Al_2(SiO_4)_{3-x}(OH)_{4x}$, was followed by ^{27}Al and ^{29}Si NMR spectroscopies. Si/OH ratios were determined from the quantitative analysis of ^{27}Al MAS–NMR components associated with $Al(OH)_6$ and $Al(OSi)(OH)_5$ environments. The ^{29}Si NMR spectroscopy was also used to quantify the unreacted silica and amorphous calcium aluminosilicate hydrates formed, C–S–H and C–A–S–H for short. From ^{29}Si NMR spectra, the amount of Si incorporated into different phases was estimated. Si and Al concentrations, deduced by NMR, transmission electron microscopy, energy dispersive spectrometry, and Rietveld analysis of both X-ray and neutron data, indicate that only a part of available Si is incorporated in katoite structures.

1. Introduction

As discussed in previous works [1–3] novel unshaped refractory materials with very low additions of calcium aluminate cements and variable additions of spherical particles of silica fume are used ubiquitously in a wide range of furnace-lining applications such as steel, cement clinker production, petrochemistry, ceramics, etc. It has been shown that the main role of silica fume is to enhance the rheological properties of these materials, improving the distribution of hydration products and the pore structure of hardened concretes, which leads to more densely packed and stronger monolithic materials [1].

The critical issue of hydration of calcium aluminate cements with silica fume, in the temperature range 40–100 °C, is one of the main challenges in the castable refractory concretes field. However, the process is not yet fully understood. Indeed the few studies related to this topic indicate that silica fume reacts with the calcium aluminate phases and water to form crystalline hydrates such as $Ca_3Al_2(SiO_4)_y(OH)_{12-4y}(0<y<3)$ (katoite) [4–7], non-crystalline and metastable phases like $Al(OH)_3$ and poorly crystalline calcium silicate hydrates and calcium aluminosilicate hydrates, denoted hereafter C–S–H and C–A–S–H for short [8,9]. Nevertheless, the extent of Si substitution in the stable hydrogarnet, katoite, has not yet been quantified.

Most cementitious phases are poorly crystallized; from this fact, the X-ray powder diffraction (XRD) cannot provide structural information. On the other hand, ^{27}Al and ^{29}Si NMR spectroscopies are useful techniques to analyze the atomic coordination and polyhedral polymerization in crystalline and amorphous materials. In both cases, from the analysis of NMR spectra, information about atoms coordination, polyhedra polymerization and first cation neighbors can be deduced [4].

In this paper, the incorporation of Si into the katoite's structure during the hydration of $Ca_3Al_2O_6$ (C_3A for short), $Ca_{12}Al_{14}O_{33}$ ($C_{12}A_7$ for short) and $CaAl_2O_4$ (CA for short) phases has been investigated. In particular, structural sites occupied by Al and Si in hydrogarnets $Ca_3Al_2(SiO_4)_{3-x}(OH)_{4x}$ ($0\leqslant x\leqslant 2.67$) have been analyzed by ^{27}Al and ^{29}Si magic-angle spinning–nuclear magnetic resonance (MAS–NMR) spectroscopies. Analytical values deduced by NMR are compared with those deduced by transmission electron microscopy (TEM) fitted with energy X-ray dispersive spectroscopy (EDS), neutron and X-ray diffraction (ND and XRD, respectively) techniques.

* Corresponding author. Fax: +34 91 735 58 43.
E-mail address: aaza@icv.csic.es (A.H. de Aza).
[1] On live at Centro Federal de Educão Tecnológica do Maranhão, CEP 65025-001, São Luís, MA, Brazil.

0022-4596/$ - see front matter © 2008 Elsevier Inc. All rights reserved.
doi:10.1016/j.jssc.2008.03.026

2. Experimental

2.1. Preparation and characterization of materials

Chemicals used in the solid-state synthesis of calcium aluminates were aluminum hydroxide hydrate ($Al(OH)_3 \cdot 0.949H_2O$, Aldrich, Milwaukee, WI, USA) and calcium carbonate ($CaCO_3$, Merck, Darmstaadt, Germany). Calcium aluminates, $Ca_3Al_2O_6$, $Ca_{12}Al_{14}O_{33}$ and $CaAl_2O_3$, were prepared from stoichiometric mixtures of aluminum hydroxide hydrate and calcium carbonate. The powders were attrition milled with yttrium partially stabilized zirconia balls in isopropanol, dried, isostatically pressed and heated in platinum crucibles at 1300 °C for $Ca_3Al_2O_6$, 1350 °C for $Ca_{12}Al_{14}O_{33}$ and 1400 °C for $CaAl_2O_3$, respectively. The samples were heated twice, with an intermediate grinding to ensure chemical homogeneity. Details of the method used for the synthesis of the calcium aluminates are given elsewhere [10,11]. XRD patterns of prepared compounds matched to $Ca_3Al_2O_6$, $Ca_{12}Al_{14}O_{33}$ and $CaAl_2O_4$ phases, without secondary phases (Powder Diffraction Files: 38-1429, 48-1882 and 70-0134 ICDD-2000 of ICDD data base).

Synthetic polycrystalline calcium aluminate powders were mixed with silica fume (Elkem microsilica® 983; Elken Materials, Inc., Pittsburgh, PA >98% reactive SiO_2, 150-nm amorphous microspheres) to obtain $Al(OH)_3$–$Ca_3Al_2(SiO_4)_{2.6}(OH)_{1.6}$ mixtures. Calcium aluminates and calcium aluminate–silica fume mixtures were treated with D_2O at a water/solid ratio by weight of 2, and placed in a tightly closed recipient at 90 °C. The study of deuterated products improved substantially the signal-to-noise ratio in ND experiments. Deuterated pastes were sieved to get homogeneous powders under 120 μm, and treated once more with D_2O in a closed vessel for 24 h at the same temperature. This process was repeated several times; in total the specimens were kept at 90 °C for 31 days.

The hydration products of $Ca_{12}Al_{14}O_{33}$ and $CaAl_2O_4$ contain two distinct crystalline phases, $Al(OH)_3$ and $Ca_3Al_2(OH)_{12}$, in different proportions, and the hydration of $Ca_3Al_2O_6$ only yields $Ca_3Al_2(OH)_{12}$ according to chemical reactions:

$$Ca_3Al_2O_6 + 6H_2O \rightarrow Ca_3Al_2(OH)_{12} \quad (1)$$

$$Ca_{12}Al_{14}O_{33} + 33H_2O \rightarrow 4Ca_3Al_2(OH)_{12} + 6Al(OH)_3 \quad (2)$$

$$3CaAl_2O_4 + 12H_2O \rightarrow Ca_3Al_2(OH)_{12} + 4Al(OH)_3 \quad (3)$$

The expected stoichiometry for Si-containing hydrated products is given by

$$Ca_3Al_2O_6 + 2.4SiO_2 + (6-2y)H_2O \rightarrow Ca_3Al_2(SiO_4)_y(OH)_{12-4y} + (2.4-y)SiO_2 \quad (4)$$

$$Ca_{12}Al_{14}O_{33} + 2.4SiO_2 + (15-2y)H_2O \rightarrow 4Ca_3Al_2(SiO_4)_y(OH)_{12-4y} + 6Al(OH)_3 + (2.4-y)SiO_2 \quad (5)$$

$$3CaAl_2O_4 + 2.4SiO_2 + (12-2y)H_2O \rightarrow Ca_3Al_2(SiO_4)_y(OH)_{12-4y} + 4Al(OH)_3 + (2.4-y)SiO_2 \quad (6)$$

where y stands for the amount of Si incorporated into the hydrogarnet structure.

According to these predictions, the resulting powders were analyzed by X-ray diffraction and consisted of gibbsite [12] and/or hydrogarnet [13] in samples without silica, and gibbsite and/or katoite in samples with silica fume (4)–(6) (gibbsite, hydrogarnet and katoite-Powder Diffraction Files: 33-0018, 84-1351 and 38-0368 ICDD-2000 of ICDD data base).

2.2. Diffraction measurements (XRD and ND)

XRD patterns were recorded with a graphite monochromated Cu$K\alpha$ radiation in a Kristalloflex D5000 (Siemens, Germany) diffractometer (Bragg–Brentano geometry) working at 40 kV and 30 mA. Measurements were done on samples rotating at 15 r.p.m., in the interval 10–90° (2θ); however in the range 90–130° the samples were not rotated to avoid the sample spilling. In all cases, X-ray patterns were acquired with a step/size of 0.03° and a time/step of 20 s.

Powder ND experiments were carried out using the high-resolution powder diffractometer for thermal neutrons instrument of the Swiss Spallation Neutron Source in the Paul Scherrer Institut (Villigen, Switzerland) [4]. ND patterns were recorded in high-intensity mode with $\lambda = 1.8857$ Å in the (2θ) interval 2.45–163° with a step size of 0.05°. In these experiments 5-g portions of the sample were inserted into a cylindrical stainless steel tube with an internal diameter of 10 mm and a height of 60 mm. Diffraction patterns were accumulated during ~1 h to obtain 106 monitor counts.

2.3. Transmission electron microscopy (TEM)

Microstructural analyses and phase identification were done by TEM (Hitachi–H7100, Japan) at 125 kV, with EDS analyzer (Rentec-M-series, Germany). Powdered samples were dispersed in propan-2-ol and deposited on carbon-coated copper grids.

2.4. Nuclear magnetic resonance (NMR) measurements

High-resolution MAS–NMR experiments were performed at room temperature in a Bruker AVANCE-400 spectrometer, operating at 104.26 MHz (^{27}Al signal) and 79.49 MHz (^{29}Si signal). ^{29}Si ($I = 1/2$) MAS–NMR spectra were recorded after $\pi/2$ pulse irradiation (4 μs), using a 500-kHz filter. To record satellite transitions in ^{27}Al ($I = 5/2$) MAS–NMR signals, spectra were recorded after $\pi/8$ pulse irradiation (1.5 μs), using a 1-MHz filter. In MAS experiments, powder samples were spun at 12 kHz for Al and 5 kHz for Si signals. The number of scans was 400 for silicon and 50 for aluminum. In both cases, time between accumulations was chosen to minimize saturation effects. The experimental error in peak position values was estimated as ±0.1 ppm for ^{29}Si and ±0.5 ppm for ^{27}Al.

The quantitative analysis of ^{29}Si and ^{27}Al MAS–NMR spectra was carried out with the Winfit software package (Bruker). This program allows the position, linewidth and intensity of components to be determined with a nonlinear iterative least-squares method. However, quadrupolar C_Q and η constants must be determined from ^{27}Al MAS–NMR spectra with a trial and error procedure. In this case, experimental profiles were simulated, considering second-order quadrupolar interactions, by using the DM2006 software package [14]. Chemical shift values of components were deduced after correction of second-order quadrupole effects. The relative amount of different species was calculated from central components after subtraction of the spinning sideband contribution of (1/2→3/2 and 3/2→5/2) satellites, following the procedure described by Massiot et al. [15].

3. Results and discussion

3.1. Diffraction

The end member of the katoite series $Ca_3Al_2(SiO_4)_y(OH)_{12-4y}$ ($0<y<3$) is known as hydrogarnet $Ca_3Al_2(OH)_{12}$ [6,13].

It crystallizes in the space group (S.G.) Ia3d (230) and exhibits a cubic unit cell of 12.55695 (3) Å, with $z = 8$ [6,10,16–18]. It belongs to the garnet family and it consists of a three-dimensional framework built-up of [$Al(OH)_6$] octahedra, [$Ca(OH)_8$] dodecahedra (distorted hexahedra) and empty tetrahedral [$(OH)_4$] cavities. As Si enters, a solid solution is formed and [$(OH)_4$] empty cavities are replaced by tetrahedral [SiO_4] units. This progressive substitution shrinks the crystal framework, and the cell parameter decreases linearly following the Vegard's law.

The Rietveld refinement of stable $Ca_3Al_2(SiO_4)_y(OH)_{12-4y}$–$Al(OH)_3$ hydrates was done following the guidelines proposed by Mc Cusker et al. [19] and the strategy described in a previous work [5]. A standard of NBS Si powder was mixed with specimens to determine zero displacements. The linear dependence between lattice parameters and silicon contents of katoites was considered to estimate the Si content of katoites in Rietveld refinements [20].

In analyzed samples, the Rietveld analysis of X-ray and neutron data, recorded at room temperature, were used to deduce deuterium site populations. The most relevant parameters deduced from structural refinements are collected in Table 1. In all samples, refined atomic positions, Debye–Waller factors and site occupancies were reasonable. From structural analyses carried out in this work, a relatively small amount of silicon entered into the katoite structure.

3.2. TEM results

Fig. 1 shows typical TEM images of Si-containing hydrated samples. In most cases, a significant amount of amorphous spherical particles and faceted gray crystals were detected. The composition of the cubic katoite grains $Ca_3Al_2(SiO_4)_y(OH)_{12-4y}$ ($0 \leqslant y \leqslant 0.5$), surrounded by amorphous silica spheres, was deduced by TEM–EDS. In all cases, the amount of silicon, deduced from Rietveld analyses of katoite's patterns, was lower than nominal values and lower than that deduced from TEM analysis (see Table 1). The apparent discrepancies can be explained if local TEM microanalyses were investigated. In these analyses, a considerable amount of silica particles was detected; part of silica was dissolved to form part of amorphous calcium aluminosilicate hydrates C–S–H and C–A–S–H. For that, an NMR study was judged to be necessary.

3.3. NMR results

3.2.1. ^{27}Al MAS–NMR spectroscopy

In Fig. 2, ^{27}Al ($I = 5/2$) MAS–NMR spectra of prepared calcium aluminates are shown. The central components (transition $1/2 \leftrightarrow -1/2$ transition) of ^{27}Al MAS–NMR spectra of $Ca_3Al_2O_6$, $Ca_{12}Al_{14}O_{33}$ and $CaAl_2O_4$ display asymmetrical signals, in the 80–90-ppm range, corresponding to different tetrahedral aluminum configurations. Spectral information deduced from ^{27}Al MAS–NMR spectra is in good agreement with that already published [21–24].

Tetrahedral distortions have been investigated taking into account the parameters Δd and $\Delta\theta$ deduced from crystallographic data, following expressions given by Ghose [25]:

$$\Delta d = \sum |\ln(d_i/d_0)| \quad (7)$$

$$\Delta\theta = \sum |\tan(\theta_i/\theta_0)| \quad (8)$$

where d_0 and θ_0 are average distances and angles, and d_i and θ_i are individual values. An analysis of distortions is given in Table 2. In

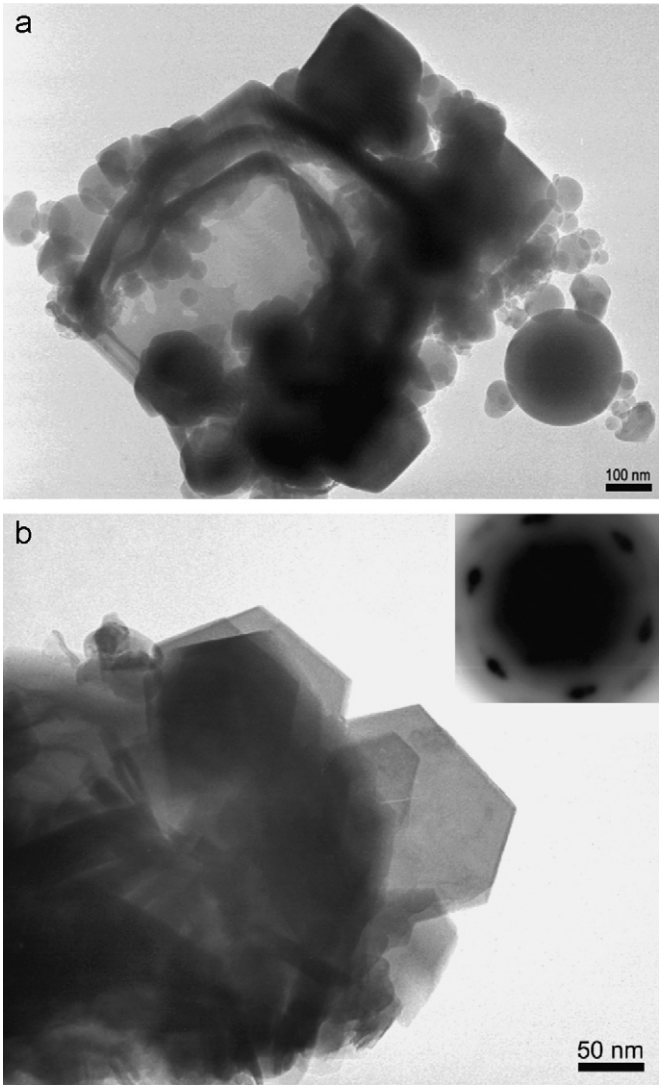

Fig. 1. Typical TEM micrographs of (a) $CaAl_2O_4$–SiO_2 mixtures, after 31 days of hydration at 90 °C, showing katoite crystallites, surrounded by unreacted silica fume nanospheres and (b) gibbsite crystals.

Table 1
Structural parameters deduced from XRD patterns of katoite

Hydration reaction	Hydrated phases identified by XRD and TEM– EDS	T/t (°C)/(h)	XRD data for katoite by Rietveld analysis		
			Lattice parameter (Å)	Occupancy of Silicon	H
3	$Ca_3Al_2(OH)_{12}$	65/168	12.5748 ± 0.0004	0.0	12.0
6	$Ca_3Al_{2.0}(SiO_4)_{0.2}(OH)_{11.2}$, Am.	90/744	12.4947 ± 0.0015	0.334 ± 0.002	10.69 ± 0.51
4	$Ca_3Al_{2.0}(SiO_4)_{0.2}(OH)_{11.2}$, 4 $Al(OH)_3$, Am	90/744	12.5248 ± 0.0029	0.190 ± 0.009	11.24 ± 0.04
5	4 $Ca_3Al_{2.0}(SiO_4)_{0.2}(OH)_{11.2}$, 6 $Al(OH)_3$, Am	90/744	12.5124 ± 0.0015	0.245 ± 0.009	11.02 ± 0.04

Lattice parameters, silicon and proton contents were deduced from the Rietveld analysis of XRD patterns recorded at room temperature. Am = amorphous phase.

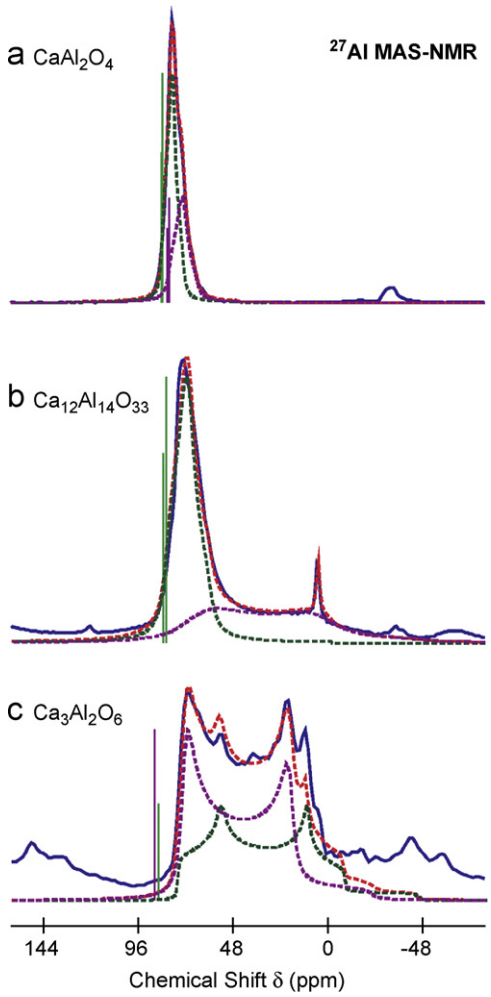

Fig. 2. Deconvolution of central components of ^{27}Al MAS–NMR spectra of (a) $CaAl_2O_4$ (CA), (b) $Ca_{12}Al_{14}O_{33}$ ($C_{12}A_7$) and (c) $Ca_3Al_2O_6$ (C_3A). The continuous line corresponds to the experimental profile and doted lines to individual components. Isotropic chemical shift values corrected from quadrupolar coupling effects are indicated by vertical lines.

general, Δd and $\Delta\theta$ increase with distortions of Al polyhedra (Al–O distances and Al–O–Al angles). These distortions are responsible for differences observed on quadrupole constants deduced from ^{27}Al MAS–NMR spectra. Results deduced in this analysis agree with those previously reported [21–24].

3.2.1.1. $CaAl_2O_4$. Hörkner and Müller [26] determined the crystal structure of $CaAl_2O_4$. The monoclinic unit cell (S.G. P21/N (14)) has $a = 8.70$ Å, $b = 8.092$ Å, $c = 15.191$ Å and $\beta = 90.17$ parameters. These authors describe the three-dimensional network as constituted by Al tetrahedra, forming six-membered rings like in tridymite structure. The crystal structure of $CaAl_2O_4$ displays six tetrahedral Al sites that have been grouped into two types for NMR interpretation purposes (Table 2).

The spectrum of $CaAl_2O_4$ (Fig. 2(a)) displays an asymmetrical signal centered at 80 ppm that corresponds to tetrahedral aluminum (denoted $A1^{IV}$). However, a careful analysis of the central transition of ^{27}Al MAS–NMR spectra shows the presence of two components. Taking into account the quadrupolar spinning-sideband pattern, two components with similar quadrupole coupling constants (C_Q) and asymmetry parameters (η_Q were deduced ($C_Q = 2.4$ MHz, $\eta = 0.8$ and $C_Q = 2.8$ MHz, $\eta = 0.8$). Peak positions, corrected from quadrupolar effects, gave chemical shift values near 83.5 and 80.0 ppm (Table 2). Experimental values deduced are close to C_Q, ν and δ values reported by Skibsted for six Al sites [21]. One of these values was previously reported by Müller et al. [23], δ_{iso}: 80.5 ppm ($C_Q = 2.7$ MHz, $\eta_Q = 0.85$).

3.2.1.2. $Ca_{12}Al_{14}O_{33}$. This compound displays the cubic crystal structure, S.G. I-43d (22), with $Z = 2$ and $a = 15.263$ Å, reported by Bartl and Séller [27]. Aluminum atoms are located in two crystallographic sites, one at the center of a regular tetrahedron and the other in slightly distorted tetrahedra. In agreement with this information, the spectrum of $Ca_{12}Al_{14}O_{33}$ (Fig. 2(b)) displays a signal at 80 ppm and a shoulder at 82 ppm, both corresponding to tetrahedral aluminum (denoted Al^{IV}). Considering the whole spectrum, two components with different quadrupole coupling constants and asymmetry parameters (η) were resolved ($C_Q = 8.7$ MHz, $\eta = 0.2$ and $C_Q = 3.5$ MHz, $\eta = 0.8$). Chemical shift values corrected from quadrupolar effects give 85.0 and 82.2 ppm

Table 2
Distortions of aluminum polyhedra

Calcium aluminate	Structural parameters					NMR parameters			
	Site	d_0 (Å)	θ_0 (deg)	Δd (Å)	$\Delta\theta_0$ (deg)	δ_{iso} (ppm) (±0.5)	C_Q (MHz) (±0.2)	η_Q (±0.1)	Fraction (%)
$CaAl_2O_4$	$Al^{IV}(1)$	1.751	109.2	0.0121	0.53	80.0	2.8	0.8	40
	$Al^{IV}(4)$	1.748	109.5	0.0147	0.22				
	$Al^{IV}(2)$	1.747	109.3	0.0057	0.39	83.5	2.4	0.8	60
	$Al^{IV}(3)$	1.765	109.4	0.0061	0.38				
	$Al^{IV}(5)$	1.753	109.4	0.0075	0.30				
	$Al^{IV}(6)$	1.756	109.3	0.0041	0.41				
$Ca_{12}Al_{14}O_{33}$	$Al^{IV}(1)$	1.748	107.3	0.0359	0.72	85.0	8.7	0.2	57
	$Al^{IV}(2)$	1.719	109.2	0.0000	0.62	82.2	3.5	0.8	43
$Ca_3Al_2O_6$	$Al^{IV}(1)$	1.751	109.4	0.0369	0.55	88.0	8.0	0	57
	$Al^{IV}(2)$	1.754	109.5	0.0148	0.66	86.0	8.7	0.3	43
$Ca_3Al_2(OH)_{12}$	$Al^{VI}(1)$	1.908	90.0	0.0000	0.00	12.4	0.7	0	100
$Al(OH)_3$	$Al^{VI}(1)$	1.902	90.2	0.0743	1.087	8.1	4.7	1	50
	$Al^{VI}(2)$	1.905	90.2	0.0871	1.121	−1.6	2.2	0.75	50

Δd and $\Delta\theta$ were calculated from structural data with Eqs. (7) and (8) of the text. NMR parameters: C_Q, quadrupolar constant; η, asymmetry parameter; δ_{iso}, isotropic chemical shift deduced from ^{27}Al MAS spectra of calcium aluminates, hydrogarnet ($Ca_3Al_2(OH)_{12}$) and gibbsite ($Al(OH)_3$). Relative proportions of Al in different deduced phases.

(Table 2). These values were similar to those reported by Skibsted et al. [21] at 85.9±1.0 ppm ($C_Q = 9.7 \pm 0.2$ MHz, $\eta = 0.4 \pm 0.1$) and 80.2±0.3 ppm ($C_Q = 3.8 \pm 0.2$ MHz, $\eta = 0.7 \pm 0.1$). One of these values was reported by Müller et al. [23] at 79 ppm ($C_Q = 3.7$ MHz, $\eta = 0.9$). Small differences detected in ^{27}Al NMR spectra of two Al signals suggest the presence of similar distortions for two tetrahedral Q^2 environments.

The sharp line at 4.7 ppm, ascribed to octahedral Al, was attributed to the presence of small amounts of an amorphous secondary phase not detected by XRD.

3.2.1.3. $Ca_3Al_2O_6$. The crystal structure for $Ca_3Al_2O_6$ is cubic, S.G. Pa3 (205) with $Z = 24$ and $a = 15.263$ Å. According to Mondal and Jeffery, the structure is formed by rings of six AlO_4 tetrahedra (Al_6O_{18}), with Ca^{2+} ions holding rings together [28].

$Ca_3Al_2O_6$ (Fig. 2(c)) exhibits a spectrum with a broad signal centered at ~40 ppm, which corresponds to tetrahedral aluminum (denoted $A1^{IV}$). The fitting of NMR spectrum did show the presence of two components with similar quadrupole coupling constants (C_Q) and asymmetry parameters (η) ($C_Q = 8$ MHz, $\eta = 0$ and $C_Q = 8.7$ MHz, $\eta = 0.3$). Chemical shift values corrected from quadrupolar effects are 88.0 and 86.0 ppm (Table 2). The values were near to that reported by Skibsted et al. [21,24], 79.5 and 78.3 ppm ($C_Q = 8.69 \pm 0.05$ MHz, $\eta = 0.32 \pm 0.02$ and $C_Q = 9.30 \pm 0.05$ MHz, $\eta = 0.54 \pm 0.02$). One of these values was reported by Müller et al. [23], 85 ppm ($C_Q = 9.7$ MHz, $\eta = 0.3$). Small differences detected in ^{27}Al NMR patterns of two Al sites suggest the presence of similar distortions in both tetrahedra [21].

3.2.1.4. Calcium aluminate hydrates. ^{27}Al NMR spectra of fully hydrated samples obtained from calcium aluminates are gathered in Figs. 3 and 4. The hydration products of $Ca_{12}Al_{14}O_{33}$ ($C_{12}A_7$) and $CaAl_2O_4$ (CA) contain two crystalline phases, $Al(OH)_3$ and $Ca_3Al_2(OH)_{12}$, in different proportions. The hydration of $Ca_3Al_2O_6$ is highly exothermic and yields rapidly to the crystalline phase $Ca_3Al_2(OH)_{12}$. According to reaction schemes given by Eqs. (1)–(3), ^{27}Al NMR spectra show the elimination of tetrahedral signals of starting compounds and the detection of octahedral environments in resulting products.

The ^{27}Al MAS–NMR spectrum of $Ca_3Al_2(OH)_{12}$ is given in Figs. 3(g) and 4(c), where the central and satellite transitions are modulated by equally spaced sidebands produced by the sample rotation. In this sample, the ^{27}Al MAS–NMR spectrum exhibits a central symmetric peak at 12.35 ppm, which is due to the octahedral Al^{VI} site surrounded by 6 [OH^-] groups. The central MAS–NMR transition was slightly affected by quadrupolar interactions. The simulation of the whole spectrum permitted to deduce quadrupolar constants ($C_Q = 0.63$ MHz, $\eta = 0$) (Table 2). These values are similar to those reported in previous works [4,13,21,29,30].

The ^{27}Al MAS–NMR spectrum of hydrated $Ca_{12}Al_{14}O_{33}$ ($C_{12}A_7$) and $CaAl_2O_4$ (CA) contains two components ascribed to

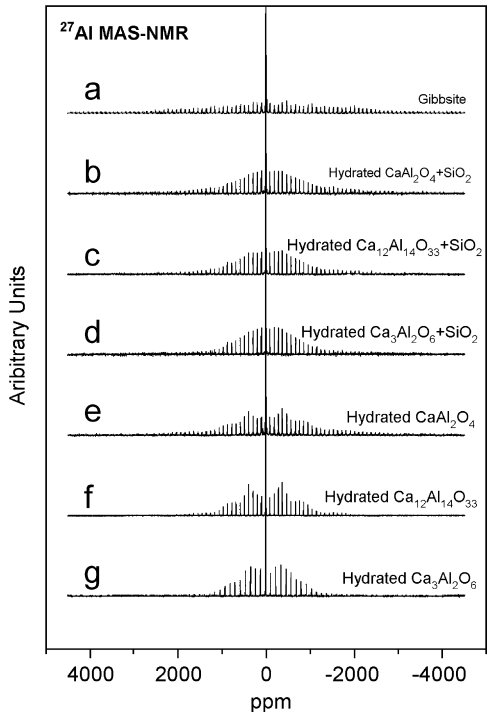

Fig. 3. ^{27}Al MAS–NMR spectra of hydrogarnet ($Ca_3Al_2(OH)_{12}$–gibbsite $Al(OH)_3$ mixtures and katoite ($Ca_3Al_2(SiO_4)_{3-x}(OH)_{4x}$)–gibbsite mixtures, produced by hydration of calcium aluminates and calcium aluminate–silica fume mixtures. In these spectra quadrupolar sideband patterns of two resulting compounds can be observed. In simulation of experimental profiles second-order quadrupolar effects have been considered (see text).

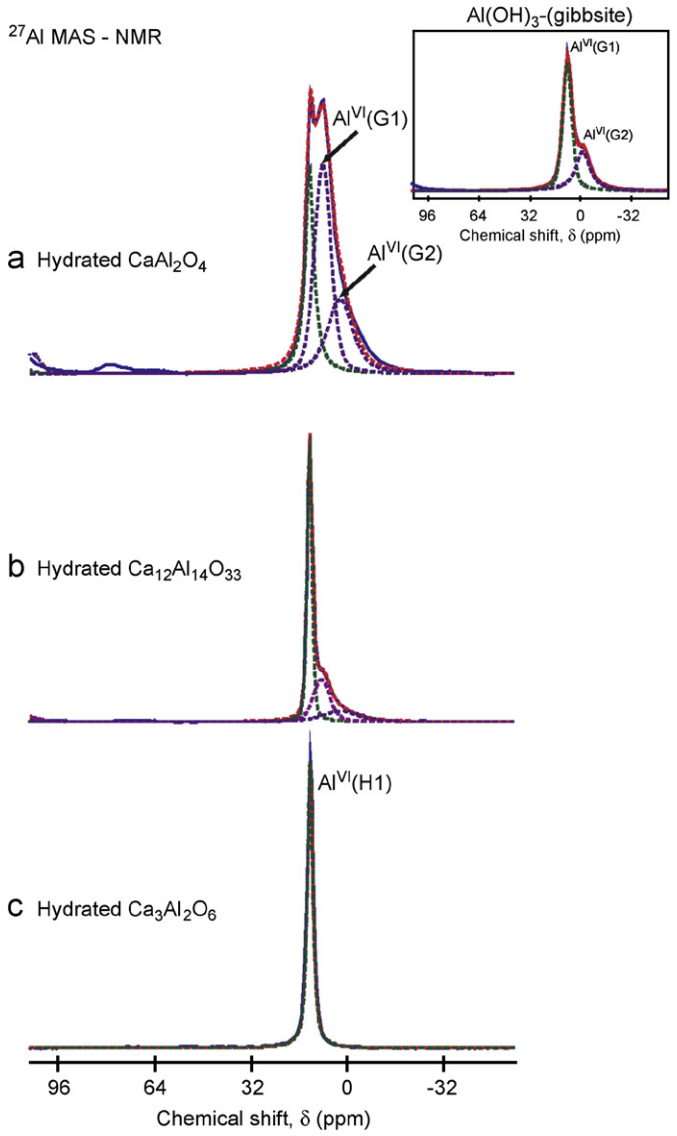

Fig. 4. Deconvolution of central components of ^{27}Al MAS–NMR spectrum of fully hydrated calcium aluminates: (a) $CaAl_2O_4$ (CA), (b) $Ca_{12}Al_{14}O_{33}$ ($C_{12}A_7$) and (c) $Ca_3Al_2O_6$ (C_3A). The continuous line corresponds to experimental profile and dotted lines to individual components. The Al^{VI}(H1) signal corresponds to Al in Katoite and Al^{VI}(G1) and Al^{VI}(G2) to Al in gibbsite (see inset).

Table 3
Chemical shift values and relative amounts of Si and Al in katoite and gibbsite phases, deduced from ^{27}Al MAS spectra of hydrates of calcium aluminates and calcium aluminate–microsilica mixtures

Hydration reaction	Hydrated phases identified by XRD	Attribution	δ_{iso} (ppm) ($\pm$0.5)	Si site occupation ($\pm$0.05)	Al fraction (%)	
					NMR	Theoretical
	$Al(OH)_3$	Al^{VI}(G1)	8.1	–	50	50
		Al^{VI}(G2)	−1.6	–	50	50
C_3A hydrated (1)	$Ca_3Al_2(OH)_{12}$	Al^{VI}(H1)	12.4	–	100	100
$C_{12}A_7$ hydrated (2)	$Ca_3Al_2(OH)_{12}$; $Al(OH)_3$	Al^{VI}(H1)	12.4	–	59	57
		Al^{VI}(G1)	8.4	–	41	43
		Al^{VI}(G2)	2.3	–		
CA hydrated (3)	$Ca_3Al_2(OH)_{12}$; $Al(OH)_3$	Al^{VI}(H1)	12.4	–	32	33
		Al^{VI}(G1)	8.4	–	68	67
		Al^{VI}(G2)	0.6	–		
C_3A+S hydrated (4)	$Ca_3Al_2(SiO_4)_{0.33}(OH)_{10.7}$	Al^{VI}(H1)	12.2	–	44	
		Al^{VI}(H2)	4.1	0.28	56	
$C_{12}A_7$+S hydrated (5)	$Ca_3Al_2(SiO_4)_{0.24}(OH)_{10}$; $Al(OH)_3$	Al^{VI}(H1)	12.2	–	60	57
		Al^{VI}(H2)	4.5	0.24		
		Al^{VI}(G1)	8.4	–	40	42
		Al^{VI}(G2)	−1.4	–		
CA+S hydrated (6)	$Ca_3Al_2(SiO_4)_{0.20}(OH)_{11.2}$; $Al(OH)_3$	Al^{VI}(H1)	12.3		32	33
		Al^{VI}(H2)	3.6	0.24		
		Al^{VI}(G1)	8.0	–	68	67
		Al^{VI}(G2)	0.9			

Al^{VI} (H)–Al in hydrogarnet; Al^{VI} (G)–Al in gibbsite.

$Ca_3Al_2(OH)_{12}$ and $Al(OH)_3$ (Fig. 3). The central component of ^{27}Al MAS–NMR spectra is given in Fig. 4. For comparative purposes the NMR spectrum of gibbsite included as an inset shows an asymmetric octahedral signal at 8.1 ppm (Fig. 4). The analysis of the whole spectrum of hydrated compounds showed the presence of three components: one signal similar to that deduced for $Ca_3Al_2(OH)_{12}$ and two corresponding to $Al(OH)_3$ [31,32]. In $Ca_3Al_2(OH)_{12}$, quadrupolar constants deduced from whole spectra were similar ($C_Q = 0.67$ MHz, $\eta_Q = 0$), indicating that formed hydrogarnets display in all samples the same structural features (see Figs. 4(a) and (b)). In agreement with 3Q-MAS experiments reported by Damodaran et al. [32], gibbsite displays two octahedral environments. Quadrupole parameters deduced for gibbsite components at 8.1 and −1.6 ppm were ($C_Q = 4.7$ MHz, $\eta = 1$) and ($C_Q = 2.2$ MHz, $\eta_Q = 0.75$), respectively (Table 2).

Bearing in mind NMR spectra of pure gibbsite and hydrogarnet, it is possible to deconvolute the central component of spectra in three components: the symmetric Al(H1) band at 12.3 ppm of $Ca_3Al_2(OH)_{12}$ and two other at 8 and −1 ppm (Al^{VI}(G1) and Al^{VI}(G2) components) corresponding to gibbsite $Al(OH)_3$ (see Figs. 4(a) and (b)). In this analysis, second-order quadrupolar patterns were used to subtract the contribution of satellite transitions to central components. From results of deconvolution, relative amounts of $Ca_3Al_2(OH)_{12}$ and $Al(OH)_3$ were deduced in each sample. These values agree with theoretical ones deduced from Eqs. (1)–(3), confirming that hydration was complete in all cases (Table 3).

Taking into account the phase equilibrium relationships within the ternary system CaO–$AlO_{1.5}$–H_2O, at 95 °C, the presence of only hydrogarnet and gibbsite, as crystalline phases, indicates that calcium aluminates are fully hydrated as could be expected for the water/solid ratio used in hydration experiments. The quantification of the Al^{VI} hydrogarnet/Al^{VI} gibbsite ratio, calculated from the ^{27}Al NMR data, matched theoretical values. According to these data, hydrated samples (water/solid = 2 at 95 °C) were located within the above-mentioned ternary system $Ca_3Al_2(OH)_{12}$+$Al(OH)_3$+H_2O (Fig. 5).

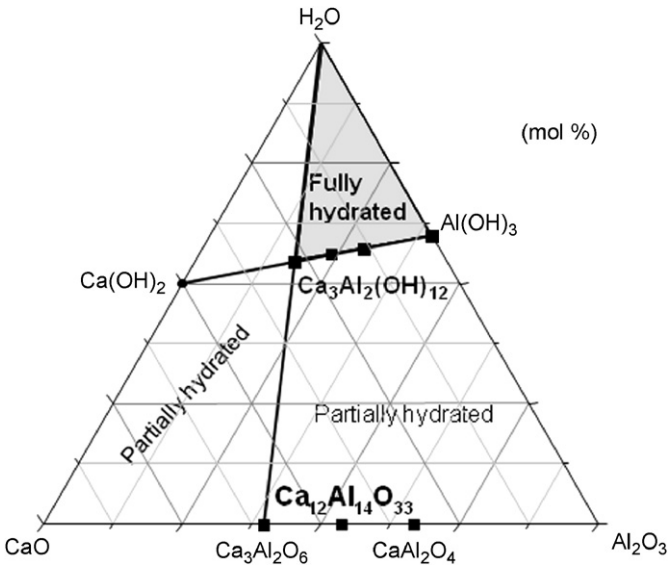

Fig. 5. Simplified sketch of the CaO–Al_2O_3–H_2O ternary system. Crystalline phase's assemblages of the CaO–$AlO_{1.5}$–H_2O ternary system, where results deduced in this work have been included.

3.2.1.5. Hydrates formed in Si-containing samples. Fig. 6 shows ^{27}Al MAS–NMR spectra of (a) $Ca_3Al_2O_6$; (b) $Ca_{12}Al_{14}O_{33}$ and (c) $CaAl_2O_4$ hydrated at 90 °C for 31 days in the presence of silica fume. In all samples, the tetrahedral Al is eliminated to give octahedral Al in hydrated samples. In Fig. 3, the whole spectra of different samples hydrated in the presence of silica fume display appreciable differences as a consequence of the presence of gibbsite and

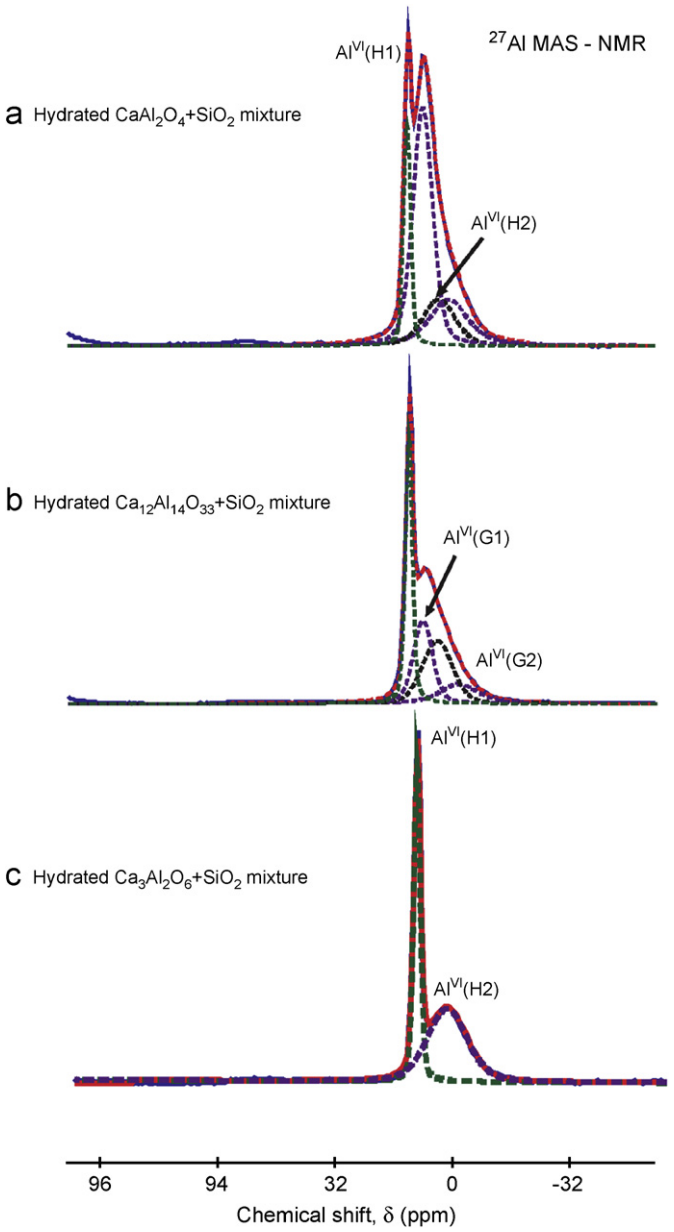

Fig. 6. ^{27}Al MAS–NMR spectrum for calcium aluminate–silica fume mixtures hydrated 31 days at 90 °C: $CaAl_2O_4$ (CA), (b) $Ca_{12}Al_{14}O_{33}$ ($C_{12}A_7$) and (c) $Ca_3Al_2O_6$ (C_3A). The continuous line corresponds to the experimental profile and dotted lines to individual components. Al^{VI}(H1) and Al^{VI}(H2) correspond to Al in hydrogarnets and Al^{VI}(G1) and Al^{VI}(G2) to Al in gibbsite.

incorporation of Si in hydrogarnet structure. The Si incorporation increases quadrupole constants of hydrogarnet ($C_Q = 0.7$ MHz, $\eta_Q = 0$) to ($C_Q = 1.1$ MHz, $\eta_Q = 0.5$) in Si-bearing katoites.

As it was described previously [5], Si enters into the katoite's structure to form the solid-solution $Ca_3Al_2(SiO_4)_{3-x}(OH)_{4x}$ ($0<x<3$). In hydrogarnets, formed in presence of silica fume, four OH^- can be substituted by [SiO_4] to form the solid-solution $Ca_3Al_2(SiO_4)_{3-x}(OH)_{4x}$. This substitution induces a perturbation on the four nearest Al neighbors of incorporated Si atoms in katoite. According to this, the appearance of the Al^{VI}(H2) band has been directly related to the formation of Al–O–Si bonds in katoites.

The amount of Si incorporated into the hydrogarnet structure has been deduced from the quantitative analysis of ^{27}Al and ^{29}Si MAS–NMR spectra (Table 4). In general, ^{27}Al MAS–NMR spectra of three hydrated aluminates display a major peak centered at 12.3 ppm and a shoulder at around 4 ppm (Fig. 6 and Table 4), associated, respectively, with octahedral Al^{VI} surrounded by 6OH (Al^{VI}(H1) signal) and Al^{VI} surrounded by 5OH and 1Si (Al^{VI}(H2) signal) in the hydrogarnet's structure [5]. In hydrated $Ca_{12}Al_{14}O_{33}$ and $CaAl_2O_4$–silica fume mixtures, two octahedral NMR components corresponding to gibbsite, designed Al^{IV}(G1) and Al^{IV}(G2), [24], were detected at 8 and 1 ppm.

^{27}Al MAS–NMR spectra were deconvoluted using second-order quadrupolar patterns. Relative amounts, deduced by subtraction of the satellite contribution from central components, coincide with those given by Eqs. (4)–(6). Taken into account that each Si shares four corners with four Al octahedra, the Si content of formed katoites can be deduced from ^{27}Al MAS–NMR spectra with the expression

$$y = 3 - x = [I\mathrm{Al(H2)}]/4$$

where IAl(H2) stands for the relative intensity of Al component ascribed to Al surrounded by 5OH,1Si. In Table 3, the amount of Si incorporated in different katoites is given. In general, it is observed that the amount of Si incorporated (0–0.33 per formula unit) is much lower than that deduced from nominal compositions, but close to that deduced by Rietveld analysis of X-ray and ND diffraction patterns.

3.2.2. *^{29}Si MAS–NMR spectroscopy*

The ^{29}Si ($I = 1/2$) MAS–NMR spectra of amorphous silica–$Ca_3Al_2(SiO_4)_y(OH)_{12-4y}$–$Al(OH)_3$ mixtures, recorded after 31 days of hydration at 90 °C, are given in Fig. 7. All hydrated samples show spectra composed of five peaks, at ~−110, −98, −87 ppm and two centered at −79 ppm (Table 4).

As a general trend, ^{29}Si chemical shift values became more negative as silicate condensation increases. That is the reason why the ^{29}Si spectrum of the amorphous silica displays a single peak at −110 ppm, associated with tetrahedral Si in Q^4[$Si(OSi)_4$] environments (Fig. 7a). In hydrated compounds, the peak at −112 ppm is quite intense, indicating that a considerable part of silica has not reacted. The other peak observed at about −99 ppm corresponds to Q^3[$Si(OSi)_3OH$] environments located at the surface of the activated silica microspheres.

The partial dissolution of silica particles produces partially depolymerized species that can capture Ca and Al ions to form Q^n species $Si(OSi)_n(OM)_{4-n}$, with $n = 1$, 2 in C–S–H phases. These species could be responsible for the broad peak detected at ~−87 ppm [33]. The broad component detected at around −79.9 ppm has been assigned to Q^0 [$Si(OAl)^{VI}_{4-x}(OCa)_x$] species, chemically bound to Ca ions in katoite's precursors (Figs. 6(b)–(d)). Finally, the narrow component detected at −79.9 ppm has been ascribed to Q^0 [$Si(OAl)_4$] environments of the hydrogarnet network, where Si shares oxygen with four neighboring $Al(OH)_6$ octahedra.

According to this assignment, and taking into account the relative intensities of different peaks, the amount of Si incorporated into katoite $Ca_3Al_2(SiO_4)_y(OH)_{12-4y}$ structure was estimated below 15% of total Si (see Table 4). On the other hand, the silica content associated with C–S–H or C–S–A–H phases, probably anchored at silica particles surface, was also deduced (peak near −87 ppm). Finally, the amount of unreacted silica fume was also deduced from the relative intensities of −110 and −99 ppm peaks, associated to Si atoms in Q^4[$Si(OSiO)_4$] and in Q^3[$Si(OSi)_3OH$] environments. Based on these determinations, most of unreacted amorphous silica (80%) remain as nanospheres, homogeneously mixed with the katoite and the amorphous phase formed during hydration processes. This model was confirmed by TEM–EDS microscopy (Fig. 1).

Until now, it was generally accepted that the main role played by silica fume was to act simply as filler, increasing the packing density in refractory castables. However, the results shown in this

Table 4
Relative amounts of Si in unreacted silica, amorphous and katoite phases, deduced from ^{29}Si MAS spectra of hydrates of calcium aluminate– silica fume mixtures

Sample	*T*/time	Particle	Chemical environment	δ_{Si} (ppm) (±0.5)	Fraction (%) (±2)
C_3A+S hydrated (4)	90/31	Amorphous silica	$Q^4(Si(OSi)_4)$	−110.5	51
			$Q^3(Si(OSi)_3\ (OH))$	−98.0	11
			$Q^2(Si(OSi)_2(OCa)_2$	−87.0	20
		Amorphous	$Q^0(Si(OAl)_{4-x}(OCa)_x)$	−79.6	8
		Katoite	$Q^0(OAl)_4$	−79.9	10
$C_{12}A_7$+S hydrated (5)	90/31	Amorphous silica	$Q^4(Si(OSi)_4)$	−110.6	52
			$Q^3(Si(OSi)_3\ (OH))$	−99.5	15
			$Q^2(Si(OSi)_2(OCa)_2$	−87.0	11
		Amorphous	$Q^0(Si(OAl)_{4-x}(OCa)_x)$	−79.6	10
		Katoite	$Q^0(OAl)_4$	−79.6	12
CA+S hydrated (6)	90/31	Amorphous silica	$Q^4(Si(OSi)_4)$	−110.5	40
			$Q^3(Si(OSi)_3\ (OH))$	−100.5	24
			$Q^2(Si(OSi)_2(OCa)_2$	−88.0	16
		Amorphous	$Q^0(Si(OAl)_{4-x}(OCa)_x)$	−79.3	8
		Katoite	$Q^0(OAl)_4$	−79.9	12
SiO_2	Unhydrated	Amorphous silica	$Q^4(Si(OSi)_4)$	−110	100

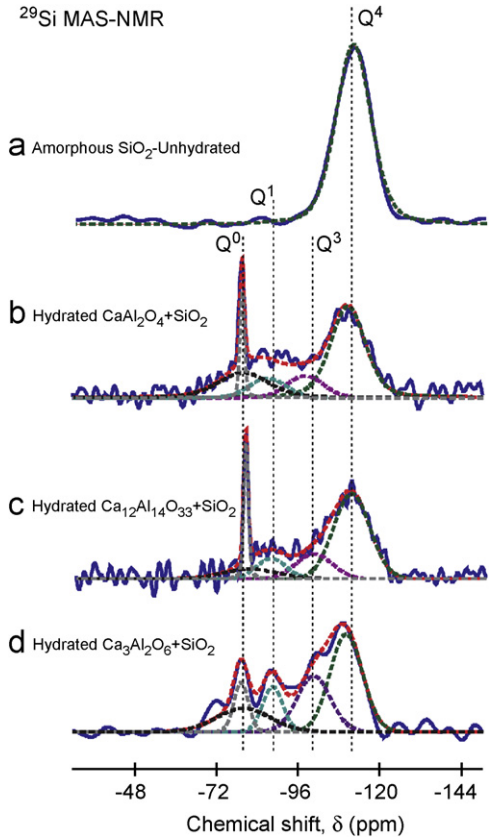

Fig. 7. Deconvolution of ^{29}Si NMR spectra of different hydrated calcium aluminosilicates–fume silica mixtures. Signals detected at −110, −100 and −89.5 ppm correspond to silica-modified particles and components at −79.9 ppm to Si incorporated in katoite structures.

paper indicate that silicon at the particle surface traps calcium ions to form interparticular amorphous C–S–H and C–A–S–H phases that enhance mechanical properties of formed refractory castables.

4. Conclusions

The suitable choice of NMR spectroscopy together with the Rietveld analysis of DRX and ND patterns allowed a better understanding of the katoites formation, during hydration of $Ca_3Al_2O_6$, $CaAl_2O_4$ and $Ca_{12}Al_{14}O_{33}$ phases in the presence of amorphous silica fume.

During hydration of calcium aluminates, tetrahedral Al (NMR component at ~80 ppm) was replaced by octahedral Al of katoite (~12 and ~4 ppm) and gibbsite (8 and −1 ppm) phases. The formation of $[SiO_4]^{4-}$ groups in katoites has been confirmed by the detection of the ^{29}Si NMR peak at −79.9 ppm ($Si(OAl^{VI})_4$ environments and of the ^{27}Al NMR peak at 3.6 ppm ($Al^{VI}(OH)5(OSi)$ environments). Both signals are indicative of the Si–O–Al^{VI} formation in the katoite's structure. The quantification of ^{27}Al and ^{29}Si NMR signals indicated that only one-tenth of SiO_2 is incorporated in formed $Ca_3Al_2(SiO_4)_{3-x}(OH)_{4x}$ katoites ($0 \leqslant x \leqslant 0.33$).

The formation of amorphous C–A–S–H species from dissolved species at the silica particle surface favors interconnection of katoite and gibssite particles and enhances mechanical properties of analyzed composites. This observation underlines the role played by silica particles in refractory castables.

Acknowledgments

This research was partially supported by MCYT under the project MAT-2006-12749-C02-01 and MAT-2004-04923-CO2-01. Neutron diffraction data were acquired at the SINQ (experiment number no II/025-18, Swiss Spallation Neutron Source-Paul Scherer Institute Villigen, Suisse). We thank Dr. D. Sheptiakov for the experimental assistance in collecting the ND data.

References

[1] W.E. Lee, W. Viera, S. Zang, K. Ghanbari Ahai, H. Sarpoolaky, C. Parr, Int. Mater. Rev. 46 (3) (2001) 145–167.
[2] J.M. Rivas Mercury, X. Turrillas, A.H. de Aza, A. Rodríguez, P. Pena, Bol. Soc. Esp. Ceram. V. 46 (6) (2007) 280–288.
[3] J.M. Rivas Mercury, A.H. de Aza, X. Turrillas, P. Pena, Bol. Soc. Esp. Ceram. V. 42 (6) (2003) 361–368.
[4] J.M. Rivas Mercury, P. Pena, A.H. De Aza, X. Turrillas, I. Sobrados, J. Sanz, Acta Mater. 55 (2007) 1183–1191.
[5] J.M. Rivas Mercury, X. Turrillas, A.H. de Aza, P. Pena, J. Solid State Chem. 179 (2006) 2988–3000.
[6] C. Cohen-Addad, P. Ducros, Acta Cryst. 23 (1967) 220–230.
[7] T.G. Jappy, F.P. Glasser, Adv. Cem. Res. 4 (1) (1991/92) 1–8.
[8] P.S. de Silva, F.P. Glasser, Cem. Concr. Res. 23 (1993) 627–639.
[9] D. Damidot, F.P. Glasser, Cem. Concr. Res. 25 (1) (1995) 22–28.
[10] J.M. Rivas Mercury, A.H. De Aza, X. Turrillas, P. Pena, J. Solid State Chem. 177 (2004) 866–874.

[11] J.M. Rivas Mercury, A.H. De Aza, P. Pena, J. Eur. Ceram. Soc. 25 (14) (2005) 3269–3279.
[12] H. Saalfeld, M. Weed, Z. Kristallogr. 139 (1974) 129–135.
[13] G.A. Larger, T. Armbruster, J. Faber, Am. Mineralog. 72 (1987) 756–765.
[14] D. Massiot, F. Fayon, M. Capron, I. King, S. Le Calvé, B. Alonso, J.-O. Durand, B. Bujoli, Z. Gan, G. Hoatson, Magn. Reson. Chem. 40 (2002) 70–76 (dmfit program).
[15] D. Massiot, C. Bessada, J.P. Coutures, F. Taulelle, J. Magn. Reson. 90 (1990) 231.
[16] R. Weiss, D. Grandjean, Acta Cryst. 17 (1964) 1329–1330.
[17] W. Dennis, J. Foreman Jr., Chem. Phys. 48 (7) (1968) 3037–3041.
[18] G.A. Lager, T. Armbruster, F.J. Rotella, G.R. Rossman, Am. Mineralog. 74 (1989) 840–851.
[19] L.B. Mc Cusker, R.B. Von Dreele, D.E. Cox, D. Louer, P. Scardi, J. Appl. Crystallogr. 32 (1999) 36–50.
[20] ICDD. International Center for Diffraction Data, Newton Square USA. ICSD Inorganic Crystal Structure Database for ICSD-for-WWW; http://icsdweb.fiz-karlsruhe.de.
[21] J. Skibsted, E. Henderson, H.J. Jakobsen, Inorg. Chem. 32 (1993) 1013–1027.
[22] J. Skibsted, H.J. Jakobsen, C. Hall, J. Chem. Soc. Faraday Trans. 90 (1994) 2095.
[23] D. Müller, W. Gessner, A. Samonson, E. Lippmaa, G. Scheler, Polyhedron 5 (3) (1986) 779–785.
[24] J. Skibsted, H. Bildsoe, H.J. Jakobsen, J. Magn. Reson. 92 (1991) 669–676.
[25] S. Ghose, T. Tsang, Am. Mineralog. 58 (7–8) (1973) 748–755.
[26] R.W. Hörkner, H.K. Müller, J. Inorg. Nucl. Chem. 38 (1976) 983–984.
[27] H. Bartl, T. Séller, Neues. Jahrb. Mineral. Monatsh. (1970) 547–552.
[28] P. Mondal, J.W. Jeffery, Acta Cryst. B 31 (1975) 689.
[29] X. Cong, R.J. Kirkpatarick, J. Am. Ceram. Soc. 76 (2) (1993) 409–416.
[30] I. Moulin, W.E.E. Stone, J. Sanz, J.-Y. Bottero, F. Mosnier, C. Haehnel, J. Phys. Chem. B 104 (2000) 9230–9238.
[31] T. Isobe, T. Watanabe, J.B. d'Espinose de la Caillerie, A.P. Legrand, D. Massiot, J. Colloid Interface Sci. 261 (2003) 320–324.
[32] K. Damodaran, P.R. Rajamohanan, D. Chakrabarty, U.D. Racherla, V. Manohar, C. Fernández, J.P. Amoreux, S. Ganapathy, J. Am. Chem. Soc. 124 (13) (2002) 3200–3201.
[33] A. Fernandez-Jimenez, F. Puertas, I. Sobrados, J. Sanz, J. Am. Ceram. Soc. 86 (2003) 1389–1394.